Supporting Information

$CsCu_{0.1}H_{2.9}PMo_{11}VO_{40}$ catalyst synthesized via a high shear mixer facilitated precipitation method for selective oxidation of methacrolein to methacrylic acid

Yanjun Li[1a], Shuai Wang [a], Qian Wang [b], Mingyuan Zhu [a], Wenjuan Shan [c], Yuanyuan Liu[* a]

[a] College of Chemistry and Chemical Engineering, Yantai University, Yantai 264005, P. R. China

[b] College of Chemistry, Chemical Engineering and Materials Science, Shandong Normal University, Jinan 250014, P. R. China

[c] College of Chemistry and Chemical Engineering, Liaoning Normal University, Dalian 116029, P. R. China

*Corresponding author

E-mail address: leeyanjun@ytu.edu.cn (Y. Li) and liuyuanyuan@ytu.edu.cn (Y. Liu)

Thermostability

The TG/DSC curves of uncalcined CP and CP-HSM samples in the 30-550 ℃ range are presented in Fig. S1. As shown in Fig. S1, three weight-losing steps, one endothermic peak, and one exothermic peak could be observed from the TG and DSC curves of these two catalysts, respectively. These three weight losing steps occurred in

[1] Corresponding author at: No. 30 Qingquan Road, Yantai 264005, China.

E-mail addresses: leeyanjun@ytu.edu.cn (Y. Li) and liuyuanyuan@ytu.edu.cn (Y. Liu)

the following order [1, 2] : (1) in the 30-200 ℃ temperature range, the absorbed water and crystal water that exists on the surface of the heteropoly anions and in the space between the heteropoly anions evaporated firstly, corresponding to the endothermic peak at 76-79 ℃; (2) Afterward, decomposition of NO_3^-, and the elimination of constitutional water which bonded to heteropoly anions or protons by certain chemical bonds started from 200 to 350 ℃; (3) At last, the catalyst began to decompose at 350 °C, and weight loss at this stage was due to the loss of the rest constitutional water (1.5 H_2O per Keggin unit) from the anhydrous salt [3]. In addition, an exothermic peak emerged at about 405 °C during this process because of the crystallization of MoO_3 [4, 5], meaning decomposition of the Keggin structure and formation of small amounts of MoO_3 [6]. For the two catalysts, their thermal decomposition behaviors were essentially the same based on the TG/DSC analysis, which suggested that the thermal stability of catalysts comes from the composition of the elements rather than the preparation method. Therefore, the same composition for the catalysts showed similar thermal stability.

Component of CsCuHPAV

The bulk elemental composition of the catalysts was obtained by ICP. The experimental and theoretical *wt.*% values of main elements in the catalysts prepared with two methods are summarized in Table S1. The general error for these elemental contents is about 2-8.5% of the calculated value except the Cu element (25% error). The low content of Cu in the catalyst is ascribed to the distinct deviation. The introduction of Cu^{2+} can accelerate the electron-transfer process in the catalytic cycle [7],

and enhance the catalytic activity (Table S2). Hydrogen content is estimated from TG analysis (Fig. S1). It can be speculated that the value is about 3 mol based on the weight loss (1.35/0.955=1.41 %) in the range of 380-450 ℃, which is close to the calculated one (2.9 mol). In addition, the absorbed water content determined by TG curve is 6 and 5 for CP and CP-HSM, respectively. These results suggest that the preparation method can achieve the synthesis of the desired stoichiometric formation of the HAPV. The elemental compositions of CP and CP-HSM are $Cs_{1.1}Cu_{0.08}H_3P_{0.98}Mo_{11.2}V_{0.86}O_{40}\cdot 6H_2O$ and $Cs_{1.07}Cu_{0.09}H_3PMo_{11.1}V_{0.94}O_{40}\cdot 5H_2O$, respectively. Thus, the difference in the bulk elemental compositions between the two catalysts can be ignored.

Effect of adding rates

The influence of addition rate was investigated for the preparations with both a conventional precipitation method and an HSM one. The microscopic images of the calcined catalysts with different addition rates for the two methods are shown in Fig. S5. It can be found that the addition rates affected the morphology of the aggregation for CP. The irregularity aggregation with the size of several micrometers can be observed at a high addition rate. With a decreased in addition rate, the morphology of the catalyst transformed into small aggregated particles with the size of several hundreds of nanometers. Compared with the CP, the influence of addition rate was smaller for CP-HSM sample, and uniform porous nanoparticles with the size of several tens were clearly detected whether at a high addition rate or a low one. On the other hand, the textural properties of the catalysts were tested to explore the influence of the

addition rate on the catalyst (Table S3). For CP, the specific surface area and intercrystallite void gradually increased with the decreasing addition rates. However, the changes in the specific surface area and intercrystallite void of CP-HSM did not follow a same rule, which closely depended on the morphology of the aggregation. Therefore, it can be concluded that for the conventional precipitation method, despite the addition rate affects aggregation behavior to a certain degree, it cannot avoid the occurrence of localized bursts of nucleation. The intensified micromixing via the HSM-assisted method is beneficial to the enhanced nucleation environment. Thus, the high surface area catalysts with uniform morphology can be prepared.

The catalytic performance of the catalysts with different addition rates was carried out, and the results are listed in Table S4. As depicted in Table S4, the differences in the conversion of MAL and the MAA selectivity are smaller for the CP and CP-HSM catalysts, respectively, which is the cause of modest changes in surface area. This emphasizes the importance of micromixing, which plays a key role in reaching high MAL conversion levels.

Effect of reaction temperature

Fig. S3 describes the effect of reaction temperature on the MAL conversion and the MAA selectivity for calcined CP and CP-HSM. The MAL conversion increased from 33.8% to 88.2% with the reaction temperature increasing within the experimental temperature range for CP. The MAA selectivity showed a volcanic trend, and the optimum reaction temperature was 320℃ with a selectivity of 79.5%. The conversion

and selectivity for CP-HSM followed the same trend. The changes in the conversion indicated that the reaction rate was accelerated with the increase in temperature, and more activated sites were involved in the reaction. The decrease of the MAA selectivity at relatively high reaction temperature resulted in further oxidation on the catalysts. Compared with calcined CP, the MAA yield for CP-HSM was high (Fig. 8c). This could be attributed to the enhanced surface morphology, a more significant amount of acid sites and increased V(IV) content in the catalyst.

Effect of reaction GHSV

The influence of GHSV on the catalytic performance of the catalysts is shown in Fig. S4. As GHSV increased, the conversion of MAL decreased first slowly in the lower range of 700-1300 h^{-1}, and then an apparent reduction was observed after 1300 h^{-1}. On the contrary, the selectivity of MAA gradually increased with the increase of GHSV. The maximum yield of MAA was reached when the GHSV was 1300 h^{-1}. The result was related to the residence time of the reactant gas in the fixed bed. In the case of lower GHSV, the residence time of the reactant gas (MAL) was longer, and thus the contact between the MAL and catalyst was adequate, resulting in the high degree of oxidation of MAL to MAA, and so was for the further oxidation. As a result, the conversion of MAL was higher, and the selectivity of MAA was lower than that in the higher GHSV. Shortening the residence time could avoid further oxidation and improve the selectivity, but the shorter contact also made the reaction unable to proceed well, resulting in a large amount of surplus MAL. Therefore, the optimum GHSV should be

1300 h^{-1} in the operational process (Fig. S4c).

Effect of mixing process on the selectivity

Changing space velocities were carried out to reach a similar MAL conversion level at the same reaction temperature. The results are gathered in Table S6. As shown in Table S6, the MAA selectivity increased from 85.7% to 92.8%, with conversion decreasing from 79% to 20% for CP-HSM, and the same trend could be found for CP. By comparison, the MAA selectivity of CP-HSM was higher by 8-15% than those of CP at similar MAL conversion levels and the various space velocities. Therefore, it is suggested that the introduction of HSM into the precipitation process could enhance the selectivity of MAA at the same MAL conversion level, and superior performance of CP-HSM could be achieved.

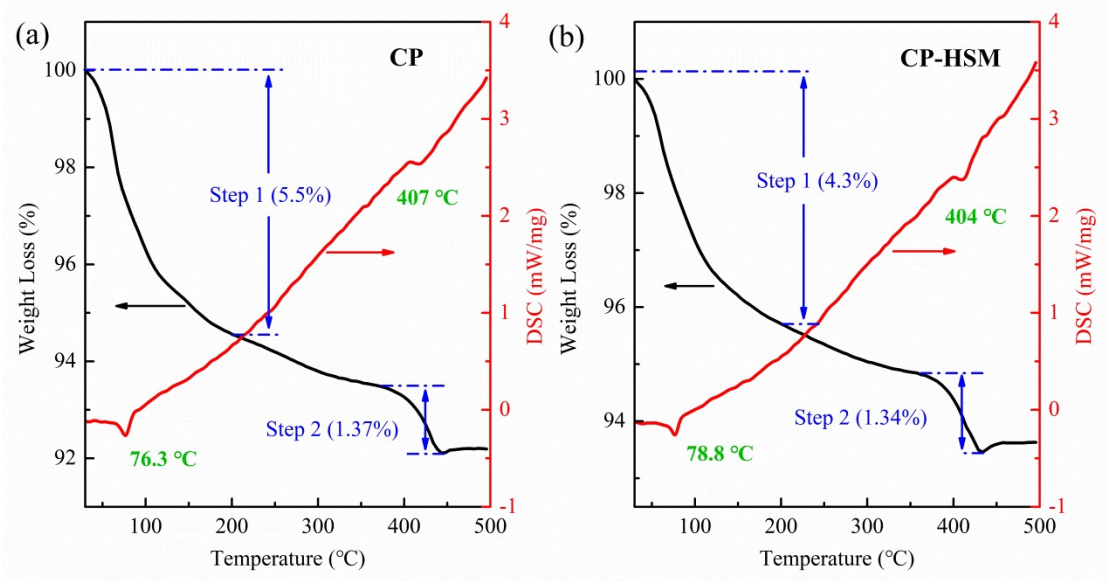

Fig. S1 TG-DSC curves of uncalcined catalysts.

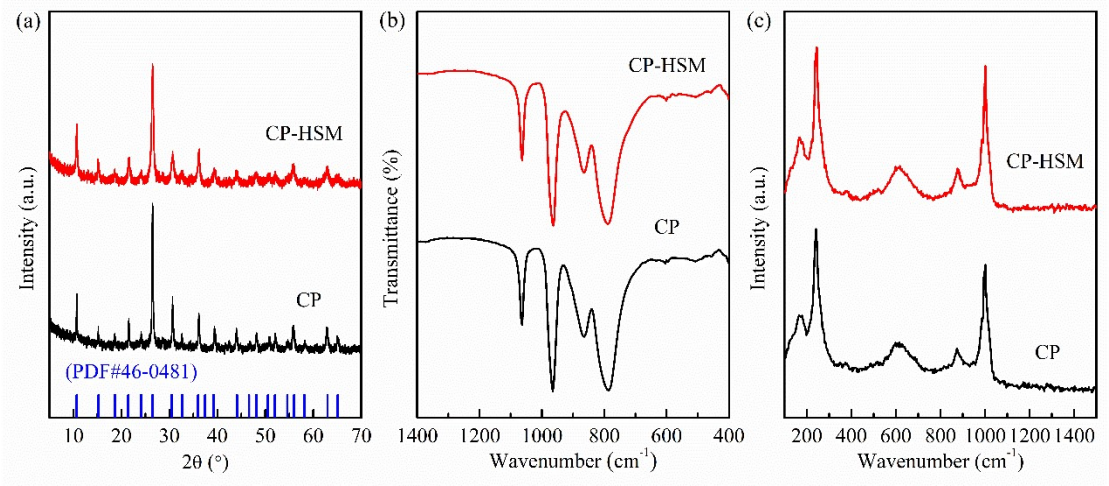

Fig. S2 XRD patterns (a), FT-IR spectra (b) and Raman spectrum (c) of uncalcined catalysts with different mixing processes.

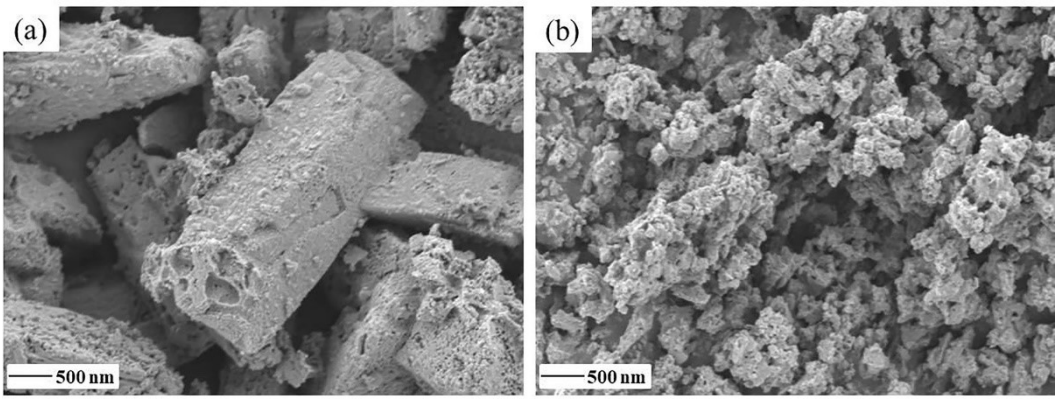

Fig. S3 The results of SEM images of uncalcined catalysts. (a) CP, (b) CP-HSM.

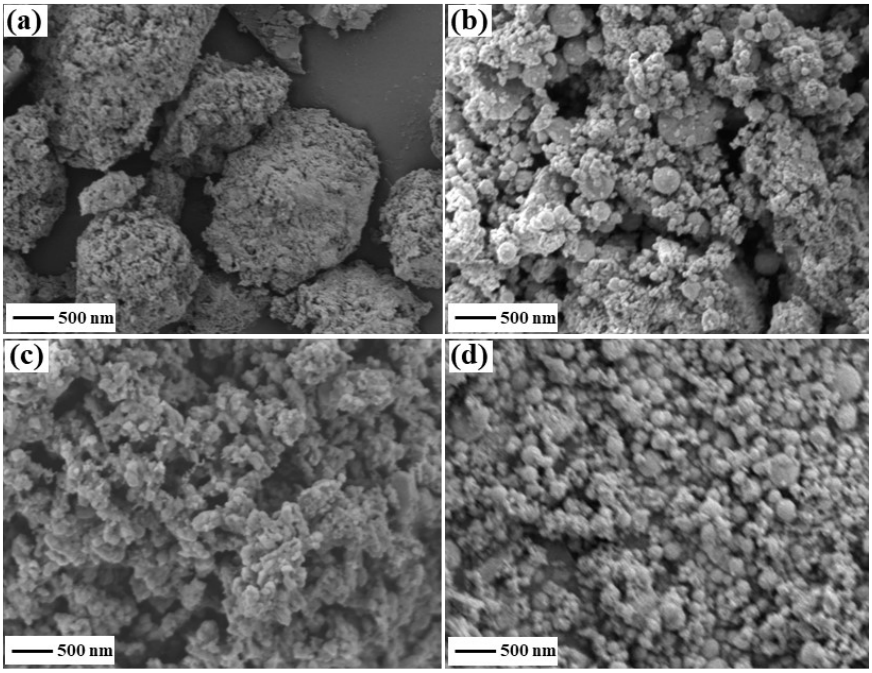

Fig. S4 SEM micrographs of the catalysts with different addition rates: (a) CP (15 ml/min), (b) CP (1 ml/min), (c) CP-HSM (15 ml/min), (d) CP-HSM (1 ml/min).

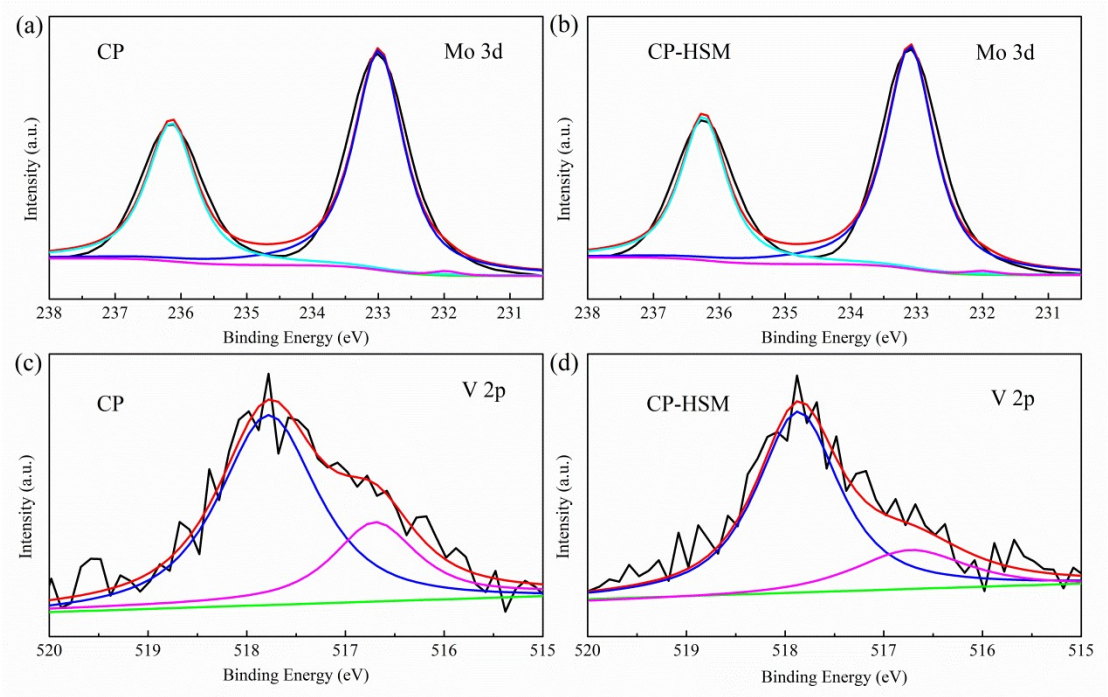

Fig. S5 XPS spectra of Mo 3d (ab) and V 2p (c-d) for uncalcined CsCuHPAV catalysts.

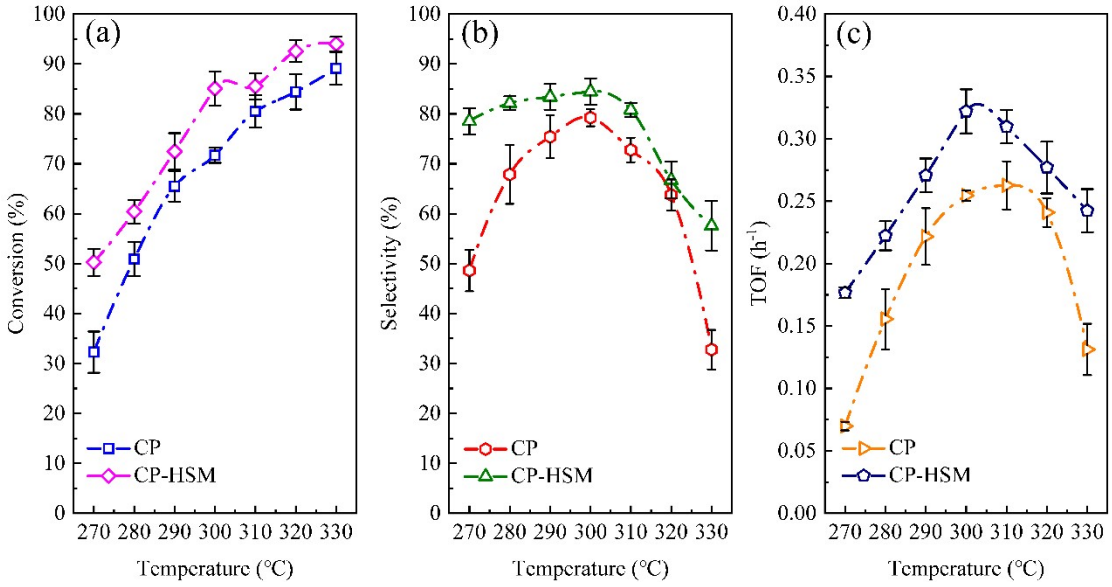

Fig. S6 Effects of reaction temperature on the performance of the CP and CP-HSM.

Reaction conditions: 12 h, GHSV=1000 h^{-1}

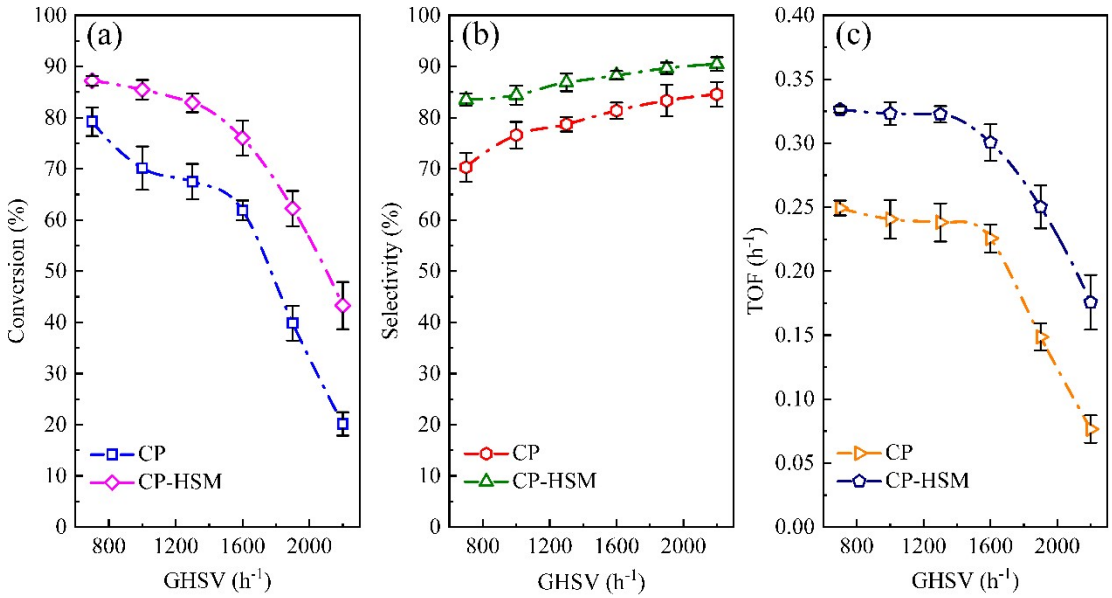

Fig. S7 Influence of GHSV on the activity (a) of MAL, selectivity (b) and TOF (c) of MAA for the CP and CP-HSM. Reaction conditions: 12 h, 300°C

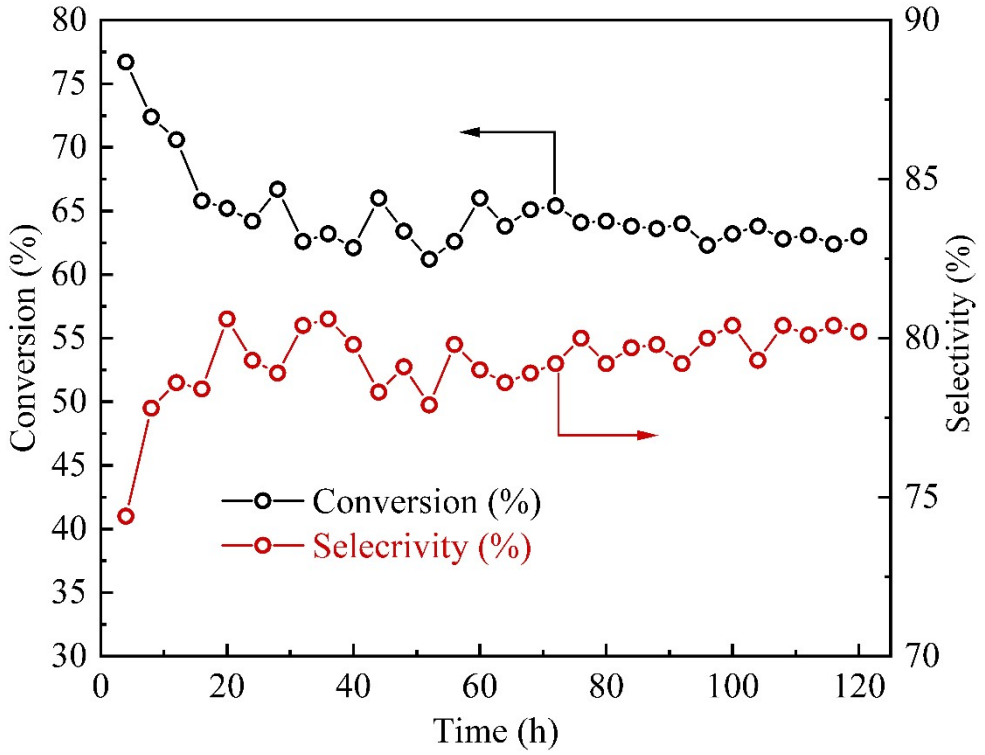

Fig. S8 The catalytic stability test over CP catalyst

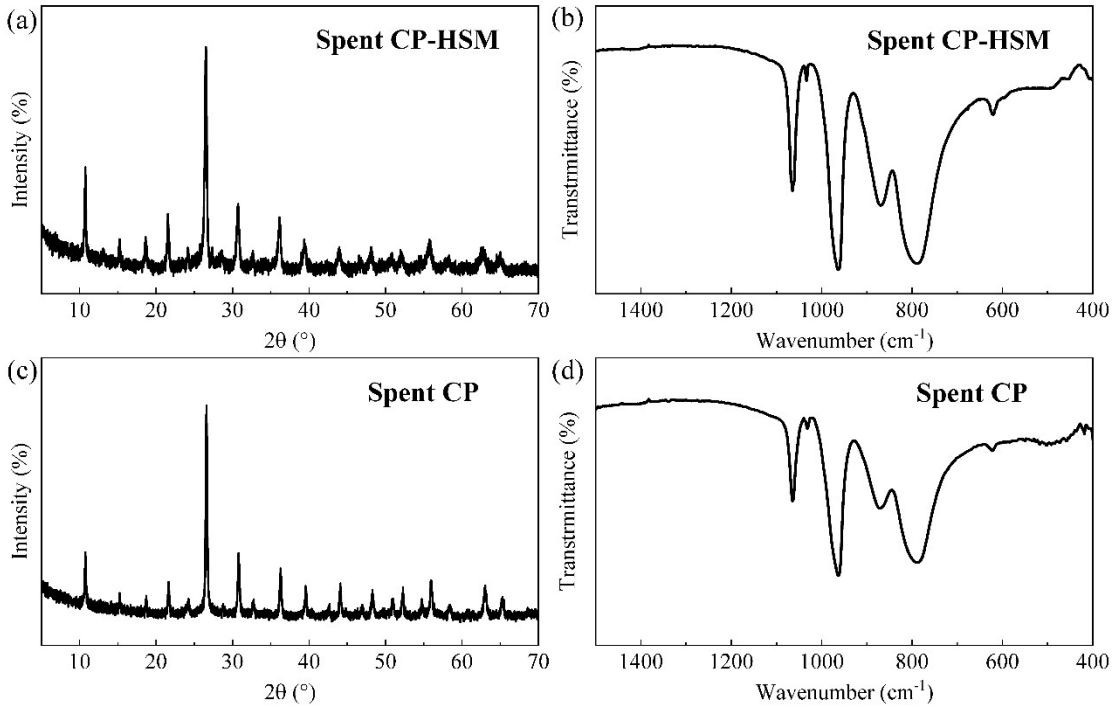

Fig. S9 XRD patterns (a, c) and FT-IR spectra (b, d) of for CsCuHPAV catalyst after the catalytic stability test.

Table S1. Bulk elemental analysis of the catalysts prepared by different methods.

Sample	Cs (*wt.*%)	P (*wt.*%)	Mo (*wt.*%)	V (*wt.*%)	Cu (*wt.*%)
CP[a]	7.51	1.56	55.17	2.41	0.25
CP-HSM[a]	7.35	1.6	55.01	2.55	0.29
CsCuHPAV[b]	6.93	1.61	54.98	2.66	0.33

[a] Experimental catalyst.

[b] Design catalyst according to the stoichiometric ratio ($CsCu_{0.1}H_{2.9}PMo_{11}VO_{40}$).

Table S2. Catalytic performance of catalysts in MAL selective oxidation

Catalyst	MAL Conv. (%)	Selec. (%)		Carbon balance (%)
		MAA	Others[b]	
CsCuHPAV[a]	85±1.2	84.9±2	8.1±1.8	95
CsHPAV[a]	76.4±2.1	84.3±1.7	8.5±2.4	93.8

Reaction condition: 300 ℃, GHSV=1000 h^{-1}, 10 g catalyst, feedstock composition of MAL/H_2O/air/N_2=3.1/15.7/8.8/72.3, time on stream=12 h, atmospheric pressure, contact time=3 s.

[a] Catalyst prepared by HSM-assisted precipitation method

[b] Other products include acetic acid, acylic acid, and CO_x.

Table S3. Textural properties of CsCuHPAV catalysts with different addition rates.

Catalysts	S_{BET}[c] (m^2/g)	Micropore area[d] (m^2/g)	Pore volume[e] (cm^3/g)	Intercrystallite void[f] (cm^3/g)
CP(15 ml/min)[a]	6.8	1.2	0.04	0.039
CP(6 ml/min)[a]	7.5	1.3	0.042	0.04
CP(2 ml/min)[a]	8.4	1.1	0.04	0.04
CP(1 ml/min)[a]	8.6	1.3	0.043	0.042
CP-HSM(15 ml/min)[b]	29.9	5.8	0.072	0.068
CP-HSM (6 ml/min)[b]	30.9	6.2	0.077	0.072
CP-HSM (2 ml/min)[b]	31.3	6.6	0.073	0.069
CP-HSM (1 ml/min)[b]	30.2	5.7	0.074	0.07

[a] Catalyst prepared by precipitation method with a conventional mixer, values in brackets indicating addition time.

[b] Catalyst prepared by HSM method, values in brackets indicate addition rate.

[c] BET surface area.

[d] Micropore area calculated by t-plot.

[e] BJH desorption cumulative volume of pores.

[f] Difference between BJH desorption cumulative volume of pores and t-plot micropore volume.

Table S4. Catalytic performance of catalysts in MAL selective oxidation

Catalyst	MAL Conv. (%)	Selec. (%)		Carbon balance (%)
		MAA	Others[c]	
CP(15 ml/min)[a]	68.9±2.1	78.6±2.5	14.6±1.7	96.8
CP(6 ml/min)[a]	71.7±1.5	79.2±1.7	12.8±2.4	94.3
CP(2 ml/min)[a]	73.6±2.2	75.9±1.6	15.7±2.1	95.4
CP(1 ml/min)[a]	72.8±1.4	80.4±1.8	10.6±1.7	92.4
CP-HSM(15 ml/min)[b]	82.3±1.3	83.6±1.7	9.3±1.1	97.2
CP-HSM (6 ml/min)[b]	85±1.2	84.9±2	8.1±1.8	95
CP-HSM (2 ml/min)[b]	84.7±1.7	84.6±1.5	8.6±1.4	93.5
CP-HSM (1 ml/min)[b]	84.3±1.6	82.9±1.8	9.7±1.2	94.5

Reaction condition: 300 ℃, GHSV=1000 h^{-1}, 10 g catalyst, feedstock composition of MAL/H_2O/air/N_2=3.1/15.7/8.8/72.3, time on stream=12 h, atmospheric pressure, contact time=3 s.

[a] Catalyst prepared by precipitation method with a conventional mixer, values in brackets indicate addition rate.

[b] Catalyst prepared by HSM method, values in brackets indicating addition time.

[c] Other products include acetic acid, acylic acid, and CO_x.

Table S5. Distribution of acidic sites and total amount of acid sites.

Catalysts	Acidity, NH_3 uptake (mmol/$g_{cat.}$)		Total acidity (mmol/$g_{cat.}$)	Surface acid density[a] (μmol/$m_{cat.}^2$)
	100-300 ℃ Weak	300-500 ℃ Medium		
CP-HSM	0.09	1.04	1.13	36.6
CP	0.07	0.71	0.78	104

[a] Acid amount per unit area, $D, \mu mol / m_{cat.}^2 = \frac{Acidity, mmol / g_{cat.}}{S_{BET}, m^2 / g_{cat.}} \times 1000$

Table S6. Comparison of the selectivities to MAA of CP-HSM and CP at a similar conversion.

Space velocity (s^{-1})		MAL Conv. (%)	MAA Selec. (%)	
CP-HSM	CP		CP-HSM	CP
0.39	0.14	79	85.7	70.3
0.5	0.28	70	88.5	76.5
0.53	0.44	62	89.6	81.8
0.61	0.51	42	90.5	82.3
0.66	0.61	20	92.8	84.5

References

[1] H. Zhang, R. Yan, L. Yang, Y. Diao, L. Wang and S. Zhang, *Ind. Eng. Chem. Res.*, 2013, 52, 4484-4490.

[2] F. Jing, B. Katryniok, F. Dumeignil, E. Bordes-Richard and S. Paul, *J. Catal.*, 2014, 309, 121-135.

[3] S. Liu, L. Chen, G. Wang, J. Liu, Y. Gao, C. Li and H. Shan, *J. Energy Chem.*, 2016, 25, 85-92.

[4] Y. Liu, S. Wang, Y. Li, X. Cai, M. Zhu and X. Han, *Appl. Catal. A Gen*, 2022, 643, 118789.

[5] V. Sydorchuk, V. Zazhigalov, S. Khalameida, J. Skubiszewska-Zięba, B. Charmas and R. Leboda, *Colloids Surf., A*, 2009, 341, 53-59.

[6] H. Kim, J. C. Jung, D. R. Park, S.-H. Baeck and I. K. Song, *Appl. Catal. A Gen*, 2007, 320, 159-165.

[7] L. Zhou, L. Wang, Y. Cao, Y. Diao, R. Yan and S. Zhang, *Mol. Catal.*, 2017, 438, 47-54.